Review of Scientific Instruments

High volume UV LED performance testing

Cite as: Rev. Sci. Instrum. **93**, 114503 (2022); https://doi.org/10.1063/5.0107372
Submitted: 04 July 2022 • Accepted: 02 November 2022 • Published Online: 16 November 2022

Benjamin C. Letson, Simon Barke, Samantha Parry Kenyon, et al.

High volume UV LED performance testing

Cite as: Rev. Sci. Instrum. 93, 114503 (2022); doi: 10.1063/5.0107372
Submitted: 4 July 2022 • Accepted: 2 November 2022 •
Published Online: 16 November 2022

View Online Export Citation CrossMark

Benjamin C. Letson,[1,a)] Simon Barke,[2] Samantha Parry Kenyon,[1] Taiwo Olatunde,[1] Guido Mueller,[2] Peter Wass,[1] Fan Ren,[3] Stephen J. Pearton,[4] and John W. Conklin[1]

AFFILIATIONS

[1] Department of Mechanical and Aerospace Engineering, University of Florida, Gainesville, Florida 32611, USA
[2] Department of Physics, University of Florida, Gainesville, Florida 32611, USA
[3] Department of Chemical Engineering, University of Florida, Gainesville, Florida 32611, USA
[4] Department of Materials Science and Engineering, University of Florida, Gainesville, Florida 32611, USA

[a)] **Author to whom correspondence should be addressed:** benletson27@gmail.com

ABSTRACT

There is increasing interest in deep UV Light-Emitting Diodes (LEDs) for applications in water purification, virus inactivation, sterilization, bioagent detection, and UV curing, as well as charge management control in the Laser Interferometer Space Antenna (LISA), which will be the first gravitational wave detector in space. To fully understand the current state of commercial UV LEDs and assess their performance for use on LISA, large numbers of UV LEDs need to be tested across a range of temperatures while operating in air or in a vacuum. We describe a new hardware system designed to accommodate a high volume of UV LED performance tests and present the performance testing results from over 200 UV LEDs with wavelengths in the 250 nm range.

I. INTRODUCTION

Existing applications for compact, solid-state UV-B and UV-C light sources in the form of deep UV (DUV) Light-Emitting Diodes (LEDs) include sterilization, water purification, medicine and biochemistry, agriculture, light sources for high-density optical memory and various curing processes.[1–3] UV-C radiation is also able to inactivate SARS-CoV-2, compromising its viral genome and virion integrity. These LEDs can be modulated at much higher frequencies than competing UV sources and feature, low noise, flexible form factors, and relatively high internal quantum efficiency.[1–3] An important basic science application will be to provide a discharge capability on the free-falling test masses within the Laser Interferometer Space Antenna (LISA), which will be the first gravitational wave detector in space.[4–7] Since these test masses will be subjected to a constant background flux of galactic cosmic rays and solar energetic particles, which result in a net positive charge on the test masses, a charge management system is needed to minimize the effect of electrostatic forces on gravitational wave observations. This charge compensation will be achieved using photoemission under illumination by ultraviolet light, which has been demonstrated several times in the past. Both Gravity Probe B[8,9] and LISA Pathfinder[10,11] demonstrated this using mercury vapor lamps, but LISA will use the new, UV-C LEDs to achieve contactless charge control in both dc and pulsed illumination schemes.[4–7]

Since testing and screening of UV LEDs for use in the LISA Charge Management Device (CMD) will be occurring at least until the CMD is integrated into the LISA spacecraft around 2030, a robust test stand is needed to allow for efficient and accurate testing of a large number of devices for years to come. The reliability of deep UV LEDs is of great current interest, especially for understanding variations between individual devices.[12–23] The test stand should be adaptable to allow for various types of measurement equipment and provide a way for the equipment to be optically coupled to the LED being tested.[3,24–27] Since many devices will be tested, the procedure for mounting an LED in the test stand should be quickly reproducible without requiring an elaborate alignment process. The test stand's final requirement is that it should be able to change the temperature of the UV LED case so that experiments can be run while simulating various environmental temperatures.

In this paper, we describe a system capable of measuring up to 96 devices simultaneously under a wide range of currents, temperatures, and dc or pulsed conditions that simulate the conditions the LEDs will encounter during the extended (4–10 years) LISA mission, but more generally one that can be used to establish the long-term reliability of these devices for any application.

II. SETUP-UV LED MOUNTING

The most important component of the UV LED test stand is the mounting piece for each device, which comprises a wedge-shaped block of Cu, called a home plate, that serves as a protective sleeve for the UV LED throughout its life cycle. Figure 1(a) shows a UV LED before it is mounted into a home plate. Since many tests will be run on these devices and they will be frequently handled, the home plate offers protection from electrostatic discharge (ESD) and contamination. The copper material was chosen to optimize the heat sinking of the LEDs as much as possible and allow for the rapid change of device temperatures within the test stand. Each UV LED is inserted into a breakout board that provides power to the devices using a micro-B universal serial bus (USB) cable, and then the UV LED is inserted into the center hole in the home plate. The breakout boards use socket-type pin receptacles that allow the UV LED to slide into place without needing to permanently attach the pins to the breakout board. This design allows the LEDs to be removed and either stored or repurposed after an initial screening process, and it preserves the integrity of the LED can and pins. After insertion, the breakout board is then fastened to the home plate, which holds the UV LED inside. Tight machining tolerances of ±0.002 in. on the home plate allow the LED to fit snugly inside, ensuring the TO-39 package is kept at thermal equilibrium with the home plate. Special ground plane utilization on the breakout board allows for optimal heat conduction from the base of the LED to the copper home plate as well.

Once a device is mounted onto a home plate, it can be inserted into a mounting block, shown in Fig. 1(b), that holds up to eight devices for simultaneous operation. This Cu mounting block can be fixed to the top of a direct-to-air thermoelectric cooler (TEC) to allow for temperature control of the devices between 20 and 80 °C. Temperature is monitored using thermistors inserted into threaded holes on the edges of the mounting block and in the center of the block on the back side. Although finite element analysis was done to ensure the temperature gradient across the mounting block was less than 1 °C, the thermistors across the back of the copper block allow for temperatures to be recorded near each LED. The wedge at the bottom of the home plate sits in a similarly shaped alignment notch in the mounting block (Fig. 2), which provides two points of contact and serves to center the home plate in each slot. Tight tolerances on the width of each slot also ensure that each home plate sits in a consistent spot each time it is inserted into the mounting block. Initial experiments measuring the effectiveness of this alignment mechanism showed that optical coupling of the LEDs was repeatable to within 1% when the home plate was inserted and removed several times.

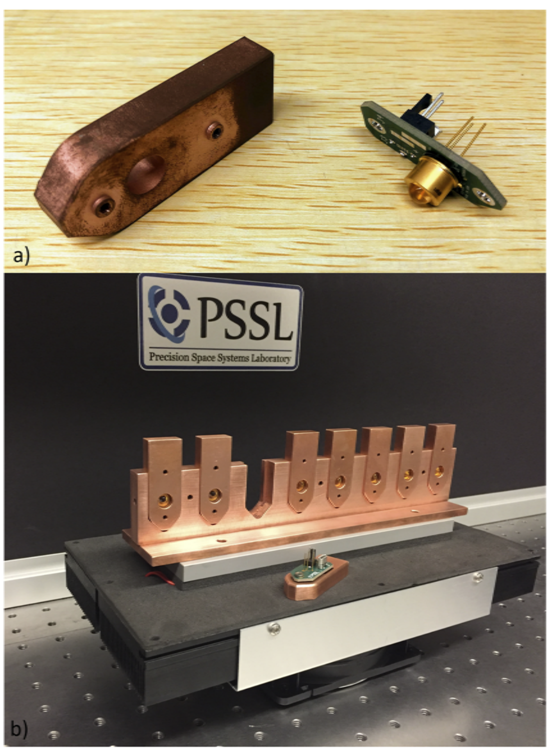

FIG. 1. (a) A UV LED mounted in its breakout board before integration into the home plate. (b) Eight UV LEDs mounted in a copper mounting block on top of the TEC. One device has been removed to show the wedge shapes used for reproducible alignment.

A. Performance rack integration

To enable testing multiple sets of eight LEDs, the Cu mounting block, temperature control unit, current driver electronics, and data acquisition hub were all integrated into a custom rack. This rack integrates all of the testing hardware into a single, semi-sealed system and provides power to the temperature controller, current driver, and power monitoring electronics. It can be closed to block out external light and provide more isolation from lab temperature fluctuations. Most importantly, multiple racks can be stacked, as

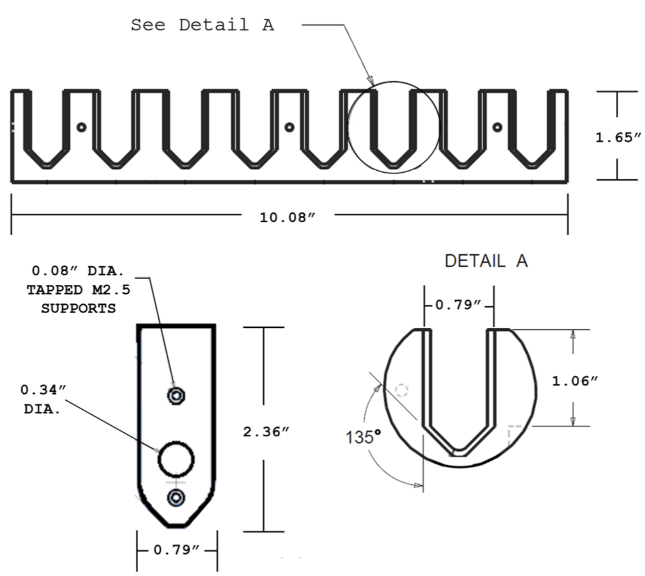

FIG. 2. Detailed drawings of the LED mounting block and home plate. The features necessary for the repeatable alignment of the LED can be seen in the drawings of both parts.

shown in Fig. 3, to enable testing of multiple sets of eight LEDs that can be run at different operating conditions.

Data acquisition and control are achieved using a National Instruments (NI) PXIe-1075 that contains 196 differential analog-to-digital converter (ADC) channels, 64 analog output channels, and eight calibrated source measurement units for continuously driving the UV LEDs. The PXIe chassis also houses an 80 MHz field-programmable gate array (FPGA) with 128 digital outputs that can be used for high frequency pulsing. The entire PXIe system is controlled by LabVIEW, which allows for control and acquisition operations to be combined into a single piece of custom software. Custom LabVIEW software is also used for the control of third-party instruments such as function generators, high-speed oscilloscopes, spectrometers, power meters, and the temperature control units used to control the temperature of the copper mounting block and home plates.

Alternatively, a custom-designed UV LED Driver Board (UVDB) connected to the DAC card (for current control) and FPGA (for pulse control) can drive up to eight LEDs simultaneously in either a pulsed or dc manner. The UVDB was designed to be a constant current source and was required to supply the UV LEDs with an adjustable current up to 100 mA and provide a compliance voltage up to 10 V via an analog voltage input. The bandwidth for this current driver must be above 100 MHz to produce sufficiently square pulses even at low duty cycles. Thus, the op amps selected as the constant current source for the UVDB have a bandwidth of 135 MHz and a maximum current output of 100 mA.

A custom board was needed to run eight UV LEDs simultaneously for the component and lifetime testing, and another three-channel board was needed to be developed toward space qualification. A total of 12 component testing boards were manufactured to lifetime test 96 UV LEDs over a number of years. The bias voltage was adjustable via a potentiometer for all eight channels of the UVDB. A connector scheme was developed for ease of integration with the NI acquisition system. The UV LEDs were connected to the UVDB via USB cables, which were selected for their robust shielding at high frequencies and for cost. The board was also equipped with two independent switching signal inputs, so that four UV LEDs could be run with a different pulsing scheme than the other four. A comparator monitored this pulsing signal and boosted its current and voltage if necessary due to digital signal losses through long cables coming from the NI FPGA. The drive currents supplied to each of the LEDs can be independently controlled via eight analog input voltages. These set voltages can be varied between 0 and 5 V, allowing the UVDB to supply drive currents between 0 and 100 mA. The UVDB allows for the acquisition of the instantaneous voltage across the UV LED as well as the average voltage and average current low-pass filtered at 1 Hz to allow for measurements of 1 s average power to be made by slower sampling acquisition systems such as the NI ADC cards. These three outputs per UV LED (24 per UVDB) can be measured through BNC connectors that could either interface with an oscilloscope for fast sampling or the NI system.

FIG. 3. Setup of the 12 LED testing racks that make up the lifetime testing wall. Each rack allows for the control of up to eight devices and provides a semi-sealed environment as the devices operate continuously for many months.

B. Focal point measurements

While the TO-39 package is less common than surface mount packages for DUV LEDs, this package is preferred for LISA because the integrated ball lens focuses the light down to a reasonable focal point, eliminating the need for additional optics to couple the light into the LISA optical fibers. To determine the optimal location for the tip of a fiber or a photodiode with a small sensitive area, measurements of the beam profile were taken of a 250 nm UV LED using a WinCam beam profiler at different drive currents and various distances from the tip of the TO-39 ball lens. After normalizing each WinCam image, rough intensity rings were identified using the first and last points from each row greater than the target intensity. Points for the 25%, 50%, 65%, and 85% intensity rings can be seen in Fig. 4(a), identified by the blue, cyan, green, and black points, respectively. A circle was then fit to the points previously identified to give an approximate diameter of the intensity ring at that distance. Images were taken at drive currents of 1, 5, and 20 mA, at distances between 5 and 15 mm away from the tip of the LED lens, and the radius from the fit for each set of points is shown in Fig. 4(b). The focal point measurements indicate that at 1 mA, the beam is still somewhat divergent, while at the drive currents above 1 mA, the focal point of the UV LED occurs at 9.75 mm from the tip of the LED irrespective of the drive current.

C. Sensing attachments

Using the information gathered from the previous experiment, an interface plate for a photodiode with a small sensitive area or fiber tip could be designed. An Ultem sensing plate was designed to perform two different measurements that require equipment to be placed precisely at the focal point of the LED, shown in Fig. 5(a). The Ultem, or polyetherimide (PEI), material was chosen to hold the sensitive electronics because it is non-electrically conducting, which will isolate the grounded cases of the eight photodiodes from one another. Ultem also possesses good machinability, low thermal conductivity, and low thermal expansion and outgasses very little under vacuum. These properties make Ultem a good choice to isolate the sensing electronics from the copper LED mounting assembly, both

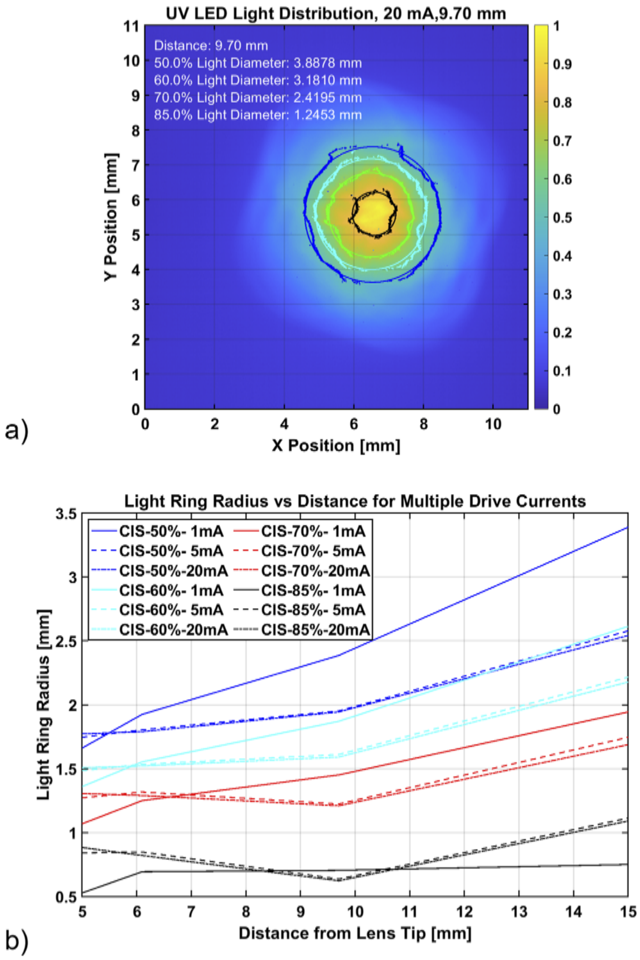

FIG. 4. Example of a WinCam image at 9.7 mm from the LED lens with four different intensity rings identified (a) and the radius of each intensity ring from multiple measurements vs distance from the LED tip (b).

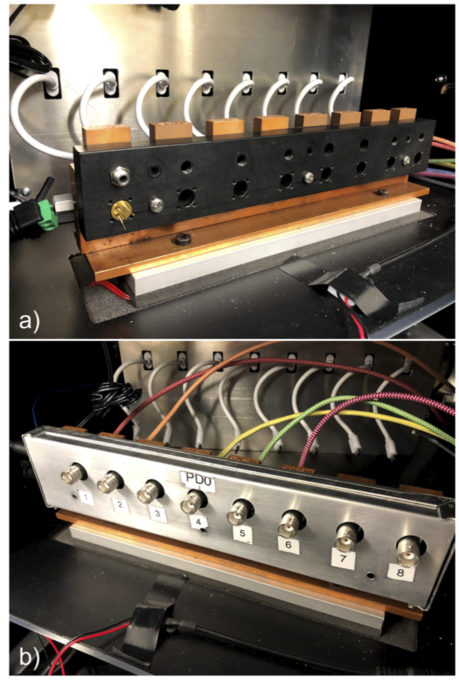

FIG. 5. Ultem sensing plate attached to the copper UV LED mounting block in the photodiode configuration (a) and LAPD sensing plate with the Faraday cage surrounding the sensitive electronics (b).

in air and in a vacuum. The interface plate can be used in two different orientations, with each orientation aligning a different sensor with the focal point of the device opposite it. In the first orientation, the UV light can be coupled into an optical fiber via an SMA-905 fiber coupler. This orientation can be used for measurements where fiber coupling is required, such as spectral measurements with a CCD spectrometer or power measurements into a fiber-coupled power meter.

In the other orientation, a TO-39 pin diode can be mounted directly into the Ultem block, which locates the photodiode lens at the LED's focal point. Therefore, the small sensitive area of the photodiode measures the most intense area of the light output. Small counterbores were added to accommodate 0.5 in. (12.7 mm) outer diameter neutral density (ND) filters that can be inserted to attenuate light or filter out longer wavelengths. A printed circuit board (PCB) is attached to the back of the sensing plate to provide power to the photodiodes and BNC connections so data can be acquired for all eight devices simultaneously.

Measurements of the total power output of an LED were made by large area photodiodes using a logarithmic trans-impedance amplifier (TIA) to amplify the photocurrent produced by the device. Since the photodiodes (Hamamatsu S1337-1010BQ) produce small photocurrents when the UV LED is operated at low drive currents, the amplifiers and supporting electronics were surrounded by a Faraday cage to prevent external signals from interfering with the sensitive measurements. The Faraday cage, large area photodiodes, and photodiode isolation plate can be seen in Fig. 5(b).

D. Vacuum chamber adaptations

While most of the UV LED tests are performed in the air, it is important to validate performance in a vacuum environment to simulate operation in space. Vacuum also allows performing tests at temperatures below the dew point without worrying about condensation affecting the LEDs or electronics.

Adaptations were made to a custom vacuum chamber, allowing for up to eight UV LEDs to be tested simultaneously at temperatures as low as $-10\,^{\circ}$C. By replacing one of the large viewing windows with a Cu disk, a Cu mounting plate could be attached vertically inside the chamber and held in place using a short support brace made from aluminum. Two-stage heating and cooling was accomplished using a Peltier device to manipulate the temperature of the Cu mounting block, while a direct-to-air TEC, similar to that used in the in-air test stand, cooled the copper disk to allow for heat generated by the Peltier unit to be removed. Graphite thermal interface material was used between all surfaces for improved thermal conductivity.

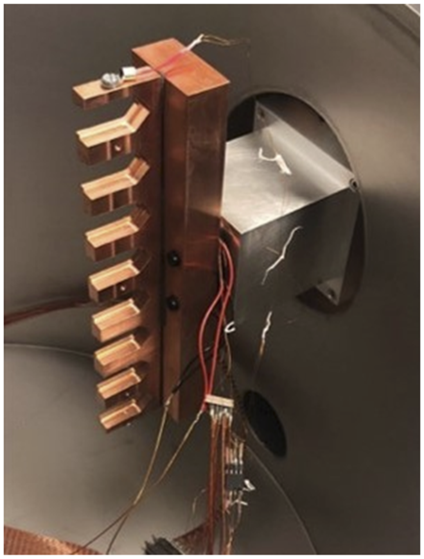

FIG. 6. Thermal vacuum adaptations made to operate up to eight UV LEDs at temperatures down to −10 °C.

Three thermistors monitor the temperature of the eight devices under vacuum. The thermistor on the top edge can be seen in Fig. 6, while there are also thermistors attached to the bottom edge and back side of the Cu mounting block. The temperature of the inside of the Cu window can also be monitored to track the system's cooling efficiency. By using the same Cu mounting piece that is used in the in-air test stand, vacuum compatible versions of the same sensing electronics can be used to either measure power in vacuum or couple light into UV fibers, which can be used to measure the optical spectrum of the device.

III. UV LED PERFORMANCE TESTS

While previous work has been done to assess the performance of UV LEDs for use onboard LISA at Imperial College London (ICL),[4,7,28] this work aims to characterize a larger number of devices over a large range of environmental temperatures. Results from two separate testing efforts are presented. In the first set of UV LED performance tests, 112 UV LEDs were initially acquired from four lots of devices manufactured by two separate vendors. These four lots are referred to as CJ, CK, SL, and SM in Table I.[29,30] After initial spectrum and current sweep measurements were made on all 112 devices at 20 °C, the eight devices with the lowest secondary emission peak and the eight devices with the highest secondary emission peak were chosen from each lot to be put through a more comprehensive set of performance tests using standard parametric testing.[3,24–27] Because the spectrum, and specifically the presence of parasitic peaks, can be interpreted as a strong indicator of the number of semiconductor defects in a device, choosing devices in this way should ensure that the performance testing devices represent both the best and worst quality devices from each manufacturing lot.

The second set of UV LED performance tests were carried out during technology readiness level (TRL) 5 verification testing of the LISA CMD. The six devices that will be presented from this testing effort were selected from a much larger batch of 120 devices from the CA and CB lots in Table I. These devices used in the TRL five CMD performance tests were selected to most closely represent the "average" device from the CA/CB lot (later referred to as TRL 5 LEDs) after initial spectrum, current sweep, and voltage sweep measurements were made on all 120 devices at 20 °C. Although the two sets of measurements were performed in different test campaigns, both sets of tests aimed to demonstrate the versatility of both the test stand and the UV LEDs themselves. The later tests on the CA and CB LEDs also give another look into how device performance can vary from one batch to the next, even among Crystal IS 250 nm LEDs.

A. Optical spectra

The first characterization measurements that were performed were measurements of the optical spectra of the devices. Optical spectrum measurements are a good indication of the recombination mechanisms occurring within the UV LED and can also give an idea of the number of semiconductor defects present within a device based on the amount of light emitted in parasitic peaks.[18,19,22,23,31] The optical spectrum of these devices is also of high importance for LISA because only light with an energy above the work function of the gold coated TM will be useful for discharging.[4–7]

The optical spectra of the initial performance devices were made at temperatures of 20, 30, and 40 °C in the performance testing rack, and temperatures of −10, 0, 10, and 20 °C in the vacuum chamber setup. The tests of the initial performance devices looked at three types of spectral measurements:

TABLE I. Device details of all five batches used in the UV LED performance tests.

Internal ID	Manufacturer	Part number	Lot number	Quantity	Nominal peak wavelength (nm)
CJ	Crystal IS	OPTAN 250J-BL	A019C1	35	250
CK	Crystal IS	OPTAN 250J-BL	A017A1	27	250
SL	SETi	TUD59H1B	⋯	25	255
SM	SETi	TCE49H1B	⋯	25	245
CA	Crystal IS	OPTAN 250J-BL	UA2001-1-1 box 1	60	250
CB	Crystal IS	OPTAN 250J-BL	UA2001-1-1 box 2	60	250

(i) A continuous, or DC, current sweep: Spectral measurements were taken at 30 logarithmic spaced currents between 0.1 and 20 mA while the LED was being driven with the NI PXIe-4140 source measurement unit.
(ii) A pulsed current sweep: Each UV LED was pulsed at 100 kHz and the duty cycle was fixed at 6%. In this test, the UV LED was driven by an eight-channel UVDB, which ramped the set current from 5 to 40 mA in eight linearly spaced steps.
(iii) A pulse duration sweep: This test examined the effect of increasing pulse duration on the spectrum of each device. Each LED was driven by an eight-channel UVDB at a constant set current of 27 mA while the pulse duration was increased from 100 ns to 2.5 μs.

In the second testing effort, optical spectrum measurements were made on the six TRL 5 devices at temperatures from −10 to + 50 °C in a large thermal vacuum chamber. The TRL 5 performance tests looked at the spectral characteristics of the devices driven in two ways, both of which used the TRL 5 Charge Management Device to power the LEDs:

(i) A continuous, or DC, current sweep: Spectral measurements were taken at 34 logarithmic spaced currents between 0.5 and 80 mA while the LED was being driven with the three-channel TRL 5 UVDB.
(ii) A pulse duration sweep: Similar to the pulse duration sweep experiment above, this test examined the effect of pulse duration on the spectral characteristics. The LEDs were pulsed at 100 kHz and a constant drive current of 20 mA. The spectrum of each device was measured at duty cycles of 5%, 10%, 15%, 20%, 25%, and 30% (pulse durations from 0.5 to 3 μs). The UV LEDs were again driven by the TRL 5 UVDB.

For both the initial performance tests and the TRL 5 performance tests, each spectrum was measured using an AvaSpec-ULS2048XL-EVO CCD spectrometer, and the light was fiber-coupled to the spectrometer with a 600 μm diameter multimode fiber optic cable.

Since the LEDs used for LISA should have the ability to be operated in both pulsed and continuous manners, both modes of operation were characterized. In the pulsed mode, the peak wavelength was found to be independent of pulse width between 100 ns and 3 μs. This corresponds to a duty cycle from 1% to 30% and none of the five lots showed a change of more than 0.1 nm over the range of duty cycles tested.

The next environmental effect that could play a role in the UV LED performance is temperature. Figure 7(a) shows the change in peak wavelength at an operating current of 20 mA over the entire temperature range tested, while Fig. 7(b) shows the change in the FWHM. The slope of the temperature dependence of peak wavelength ranged from 4.4×10^{-3} to 1.4×10^{-2} nm/°C for the different lots examined and 9.6×10^{-3} to 2.9×10^{-2} nm/°C for FWHM, corresponding to an average FWHM of ~10 nm at 20 °C. The wavelength of the main peak not only gets longer as temperature increases but the spectrum gets wider as well. Although more devices were tested in this study, these devices behave similarly to those tested previously at ICL as well.[4] The temperature dependence seen here would translate into a shift of less than 0.5 nm over the 10–40 °C operating range the devices are expected to be used in during the LISA mission.

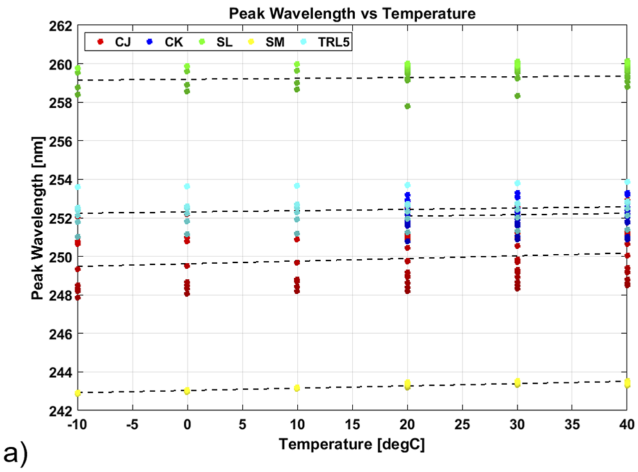

a)

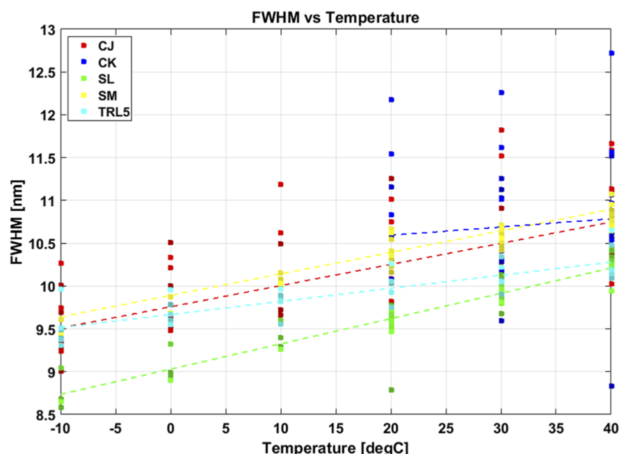

b)

FIG. 7. (a) Change in peak wavelength as a function of temperature for all performance UV LEDs. Devices were operated at a drive current of 27 mA at a constant temperature of 20 °C in air. (b) Change in the full width at half maximum (FWHM) as a function of the operating temperature for all performance UV LEDs.

B. UV power measurements

One of the main advantages of using UV LEDs over previous UV light sources such as Hg vapor lamps is the large dynamic range of UV power output achieved by operating the UV LEDs in a pulsed manner. To characterize the power output of the four lots of performance LEDs, power measurements were made on the initial 64 performance devices at temperatures of 20, 30, and 40 °C in the performance testing rack, and temperatures of −10, 0, 10, and 20 °C in the vacuum chamber setup. Again, three types of current–voltage–power (IVP) measurements were made to demonstrate the large dynamic range of the devices.

(i) A dc current sweep: While being driven by the calibrated NI-4140 source measurement unit, the LEDs were swept from 0.1 to 20 mA in 30 logarithmically spaced current steps.

(ii) A pulsed duty cycle sweep" The LED's commanded duty cycle was swept from 1% to 25% in eight logarithmic steps while the pulses per second (PPS) were held constant at 100 000.

(iii) A pulse number sweep: The LEDs were driven by the eight-channel UVDB at a constant set current of 27 mA while the duty cycle was held at 6% (0.6 μs pulse width). The pulse rate was increased from 1000 to 100 000/s in 20 logarithmically spaced steps.

Similar measurements of the UV power output were also made on the six TRL 5 LEDs at temperatures between −10 and + 50 °C in the thermal vacuum (TVAC) chamber during TRL 5 environmental testing. The main TRL 5 results presented in Fig. 8 are from a dc current sweep performed at currents ranging from 0.2 to 80 mA in 34 logarithmic steps.

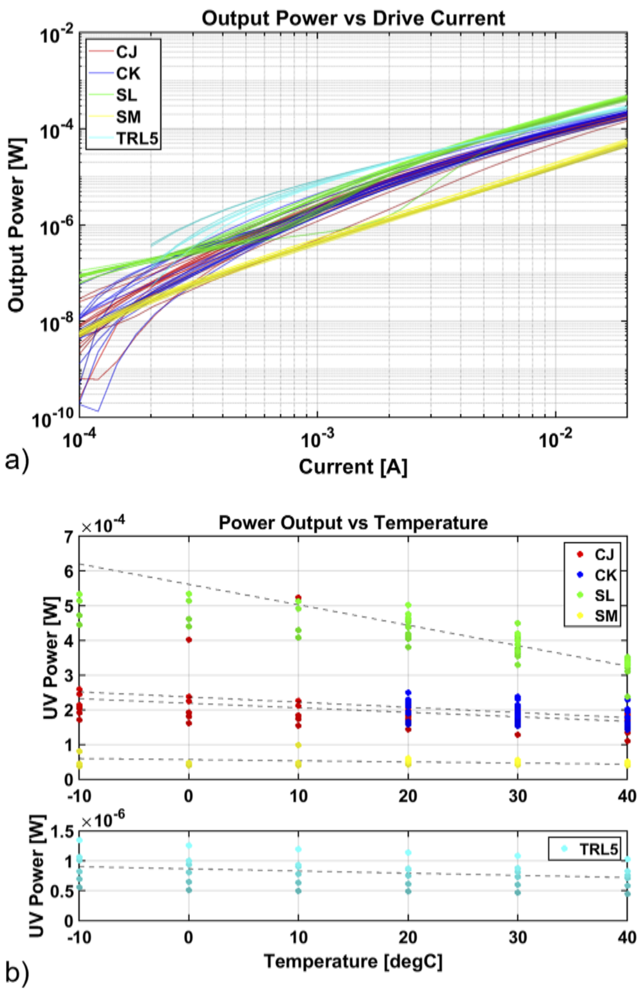

FIG. 8. (a) Change in output power as a function of drive current at 20 °C in air for all LEDs. (b) Change in output power as a function of operating temperature at 20 mA. The top plot shows the total power out of the performance LEDs while the bottom subplot shows the power measured through a fiber from the TRL 5 UV LEDs.

Figure 8(a) shows output power as a function of drive current from 0.1 to 20 mA in 30 logarithmically spaced steps. The SL and SM devices emitted around 0.4 and 0.05 mW, respectively, at 20 mA. The TRL 5 and SL devices showed good consistency across the majority of the IVP curve, but the two lots of Crystal IS (CIS) devices did show varying behavior at drive currents below 1 mA. This effect could be related to the varying spectra of the devices at low currents as well since both effects indicate the occurrence of indirect recombination as a consequence of point defects as predicted by the Shockley–Read–Hall theory.

Figure 8(a) shows how increasing the temperature of the LED leads to a decrease in the output power of each device and shows the TRL 5 LEDs on a different subplot than the other four lots due to the different measurement scheme since they were operated inside of the TVAC chamber and were fiber-coupled to photodiodes. The amplitude of the output power was reduced by a factor of ≈300 due to losses from coupling into a single core 600 μm diameter fiber and going through the TVAC feedthrough. The CJ and CK devices were all affected by temperature in a similar manner, showing a loss of ≈0.7%/°C, but the TRL 5 LEDs showed the smallest temperature impact—only losing 0.46%/°C.

Both the pulsed duty cycle and pulse per second sweep measurements showed that the output power of the device increases linearly with both of these parameters, as expected. While these performance measurements showed that the output power could be increased by two orders of magnitude by increasing the pulses per second from 1000 to 100 000, the TRL 5 performance tests were able to use a more sensitive photodiode amplifier to show that the linear relationship was constant all the way down to driving settings of less than ten pulses per second. The TRL 5 devices showed an output power dynamic range on the order of 10^7, as shown in Fig. 9, where the UV power of the device is scaled to the estimated power delivered to the LISA GRS. The horizontal axis of the plot displays the "integrated current," which is the 1 s average current delivered to the device and is computed as the product of the set current, duty cycle, and pulses per second divided by 100 000. All six UV LEDs tested were able to produce more than 500 nW in a dc driving mode, more than 125 nW in a pulsed mode, and less than 10 pW in the pulsed and quasi-DC operating modes. These benchmarks are all indicated by horizontal black dashed lines. The center of Fig. 9 is empty because the TRL 5 performance tests were constructed to specifically show the behavior at the upper and lower ranges of their output capability. The pulsed performance measurements mentioned previously showed that output power varies linearly with the number of pulses per second; so, increasing the integrated current from 1×10^{-3} to 2 mA s would show a linear increase in power that would connect the two ends of the plot.

The results of the UV LED power measurements show that the UV LEDs have a dynamic range of $\approx 10^3$ in dc mode when the drive current is increased from 0.1 to 20 mA, and the high bandwidths of the UV LEDs allows them to put out optical powers ranging over another three orders of magnitude by varying the pulse width and pulses per second over the ranges tested. The pulse width and pulses per second can be reduced to a level where the LEDs output less than 10 pW, and the power output resolution allows the average power to be controlled in increments of less than 1 pW at a driving current of 20 mA. Temperature characterization shows that most devices lose less than 1% of their output power for every degree of increase in the

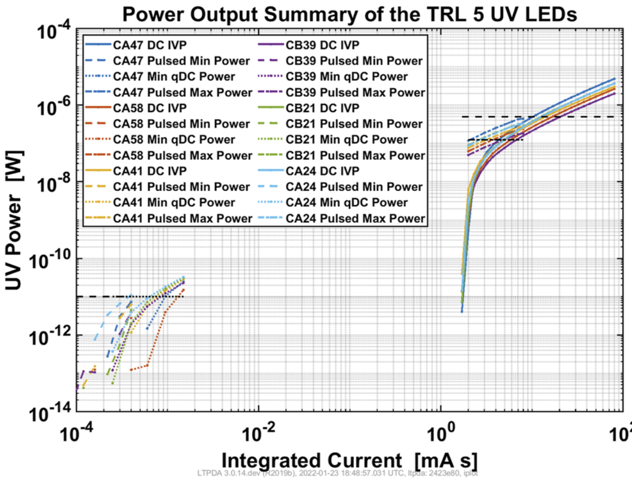

FIG. 9. Output power of the six UV LEDs used in TRL 5 CMD performance testing. The power output is shown across the entire operating condition range used to verify TRL 5 requirements.

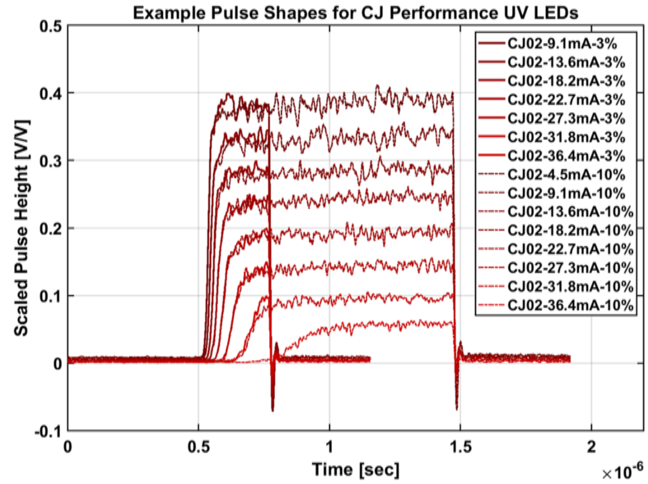

FIG. 10. Example pulse shapes from a typical CIS UV LED tested. Commanded pulse widths of 0.3 and 1 μs are shown.

operating temperature and that this trend holds for all the operating currents tested.

C. Pulse commanding characterization

The pulsed operation of UV LEDs allows for the introduction of new discharge modes relying on precisely timed UV pulses synchronized with the internal 100 kHz injection signal present within the LISA GRS. Since the pulse position with respect to the 100 kHz sinusoid directly impacts the equilibrium test mass charge,[32,33] the output of the CMD should be precisely known to allow for accurate discharging of the TM. Using a Tektronix MSO54 high-speed oscilloscope and a photomultiplier tube to amplify the UV pulses, measurements of the pulse width, rise time, and latency of the UV pulses were made while commanding a pulse width of either 300 ns or 1 μs and a phase delay of 0 μs. These measurements were made using drive currents between 4.5 and 36.5 mA and temperatures of 20–40 °C in the performance testing rack for the initial performance testing devices.

Figure 10 shows an example pulse shape ramp from a single LED. Measurements were made at driving currents between 4.5 and 36.5 mA for commanded pulse widths of 300 ns and 1 μs. The figure shows that for a given set current, the front edge of the UV pulse looks the same regardless of commanded duty cycle, and the only difference is the position of the falling edge of each pulse. As the drive current was increased, the difference between the commanded pulse and achieved pulse for the UV LEDs became smaller and the offset did not depend on the commanded duty cycle. This means that the duty cycle command can be adjusted based on the drive current only and not based on the desired duty cycle or requested latency. The pulse property measurements show that the pulse shape produced by the UV LEDs generally becomes more square at higher driving currents, and that all the LEDs from within a single batch behave similarly. These measurements also show that without any calibration, there will be slight differences between the commanded pulse shape and the achieved pulse shape. However, the measurements of pulse width and latency can be used to calibrate future flight units for LISA. Overall, the pulsing characteristics of DUV LEDs are more uniform at currents greater than 10 mA, with only a slight dependence on the operating temperature, with changes less than 1%/°C.

IV. SUMMARY AND CONCLUSIONS

We have presented the design of the ground support equipment used to protect UV LEDs throughout their lifetime and allow for ≈100 devices to be tested both in air and in vacuum over a range of operating temperatures and driving conditions to fully characterize the performance of these UV LEDs. The results of one of the most comprehensive studies of UV LED performance were also presented and show that UV LEDs are capable of performing all the tasks required by LISA and that they are more than sufficient to replace the mercury vapor lamps used for previous space missions.

The performance tests of both DC and pulsed operation and the effect of different driving conditions across the extended −10 to +40 °C operating range of LISA showed that the spectra, UV power, and pulse properties of devices even from the same lot vary widely at low drive currents. However, as the driving current is increased, the performance of the LEDs greatly improves in terms of spectrum purity, uniform power output from device to device, and more square pulse shapes. Although the drive current of the LEDs can be reduced to illuminate the test mass with less light, other methods such as pulsing the LEDs at drive currents above ≈10 mA with a reduced duty cycle or decimated number of pulses per second should be used first before running the LEDs at a low, continuous driving current.

The performance tests also showed that each lot of devices had a peak wavelength that was not exactly what the manufacturer advertised and that each lot of devices also produced a different level of

UV power. Both these characteristics have discharging implications for LISA, but the spectra of all devices fell within the 230–280 nm band of useful UV light, and all the TRL 5 devices tested were able to meet both maximum and minimum power requirements for the LISA Charge Management Device.

ACKNOWLEDGMENTS

This work was supported by NASA Grant No. 80NSSC17K0277 and NASA Contract No. 80NSSC22K0288.

AUTHOR DECLARATIONS

Conflict of Interest

The authors have no conflicts to disclose.

Author Contributions

Benjamin C. Letson: Data curation (lead); Formal analysis (lead); Software (lead); Visualization (lead); Writing – original draft (lead); Writing – review & editing (lead). **Simon Barke**: Data curation (equal); Formal analysis (equal); Investigation (equal); Methodology (equal); Software (equal); Visualization (equal). **Samantha Parry Kenyon**: Data curation (supporting); Investigation (supporting); Writing – original draft (supporting). **Taiwo Olatunde**: Data curation (equal); Investigation (equal); Supervision (equal); Validation (equal). **Guido Mueller**: Funding acquisition (supporting); Methodology (equal); Supervision (equal); Writing – review & editing (equal). **Peter Wass**: Conceptualization (equal); Funding acquisition (equal); Investigation (equal); Methodology (equal); Project administration (equal); Supervision (equal); Validation (equal); Visualization (equal). **Fan Ren**: Methodology (equal); Supervision (equal); Validation (equal). **Stephen J. Pearton**: Methodology (equal); Supervision (equal); Validation (equal); Writing – original draft (equal); Writing – review & editing (equal). **John W. Conklin**: Funding acquisition (lead); Supervision (lead); Validation (equal); Writing – review & editing (equal).

DATA AVAILABILITY

The data that support the findings of this study are available from the corresponding author upon reasonable request.

REFERENCES

[1] H. Hirayama, "Recent progress in AlGaN deep-UV LEDs," in *Light-Emitting Diode*, edited by J. Thirumalai (IntechOpen, Rijeka, 2018), Chap. 7.

[2] M. S. Shur and R. Gaska, "Deep-ultraviolet light-emitting diodes," IEEE Trans. Electron Devices **57**, 12–25 (2010).

[3] N. Trivellin, D. Fiorimonte, F. Piva, M. Buffolo, C. De Santi, G. Meneghesso, E. Zanoni, and M. Meneghini, "Reliability of commercial UVC LEDs: 2022 state-of-the-art," Electronics **11**, 728 (2022).

[4] D. Hollington, J. T. Baird, T. J. Sumner, and P. J. Wass, "Characterising and testing deep UV LEDs for use in space applications," Classical Quantum Gravity **32**, 235020 (2015).

[5] P. J. Wass, H. M. Araújo, D. N. A. Shaul, and T. J. Sumner, "Test-mass charging simulations for the LISA pathfinder mission," Classical Quantum Gravity **22**, S311–S317 (2005).

[6] S. Saraf, S. Buchman, K. Balakrishnan, C. Y. Lui, M. Soulage, D. Faied, J. Hanson, K. Ling, B. Jaroux, B. A. Suwaidan, A. AlRashed, B. Al-Nassban, F. Alaqeel, M. A. Harbi, B. B. Salamah, M. B. Othman, B. B. Qasim, A. Alfauwaz, M. Al-Majed, and D. DeBra, "Ground testing and flight demonstration of charge management of insulated test masses using UV LED electron photoemission," Classical Quantum Gravity **33**, 245004 (2016).

[7] P. Wass and LISA Pathfinder Collaboration, "Free-fall performance for the LISA gravitational wave observatory: New results from LISA pathfinder," in *APS April Meeting 2018* (2018), Vol. 2018, p. C14.001. Available at http://meetings.aps.org/link/BAPS.2018.APR.C14.1 (accessed on 1/12/2021).

[8] S. Buchman, W. Bencze, R. Brumley, B. Clarke, and G. M. Keiser, "The design and testing of the Gravity Probe B suspension and charge control systems," AIP Conf. Proc. **456**, 178–187 (1998).

[9] J. W. Conklin and Gravity Probe B Collaboration, "The Gravity Probe B experiment and early results," J. Phys.: Conf. Ser. **140**, 012001 (2008).

[10] R. Dolesi, D. Bortoluzzi, P. Bosetti, L. Carbone, A. Cavalleri, I. Cristofolini, M. DaLio, G. Fontana, V. Fontanari, B. Foulon, C. D. Hoyle, M. Hueller, F. Nappo, P. Sarra, D. N. A. Shaul, T. Sumner, W. J. Weber, and S. Vitale, "Gravitational sensor for LISA and its technology demonstration mission," Classical Quantum Gravity **20**, S99–S108 (2003).

[11] M. Armano, H. Audley, G. Auger, J. Baird, P. Binetruy, M. Born, D. Bortoluzzi, N. Brandt, A. Bursi, M. Caleno, A. Cavalleri, A. Cesarini, M. Cruise, K. Danzmann, I. Diepholz, R. Dolesi, N. Dunbar, L. Ferraioli, V. Ferroni, E. Fitzsimons, M. Freschi, J. Gallegos, C. G. Marirrodriga, R. Gerndt, L. I. Gesa, F. Gibert, D. Giardini, R. Giusteri, C. Grimani, I. Harrison, G. Heinzel, M. Hewitson, D. Hollington, M. Hueller, J. Huesler, H. Inchauspé, O. Jennrich, P. Jetzer, B. Johlander, N. Karnesis, B. Kaune, N. Korsakova, C. Killow, I. Lloro, R. Maarschalkerweerd, S. Madden, D. Mance, V. Martín, F. Martin-Porqueras, I. Mateos, P. McNamara, J. Mendes, L. Mendes, A. Moroni, M. Nofrarias, S. Paczkowski, M. Perreur-Lloyd, A. Petiteau, P. Pivato, E. Plagnol, P. Prat, U. Ragnit, J. Ramos-Castro, J. Reiche, J. A. R. Perez, D. Robertson, H. Rozemeijer, G. Russano, P. Sarra, A. Schleicher, J. Slutsky, C. F. Sopuerta, T. Sumner, D. Texier, J. Thorpe, C. Trenkel, H. B. Tu, D. Vetrugno, S. Vitale, G. Wanner, H. Ward, S. Waschke, P. Wass, D. Wealthy, S. Wen, W. Weber, A. Wittchen, C. Zanoni, T. Ziegler, and P. Zweifel, "The LISA pathfinder mission," J. Phys.: Conf. Ser. **610**, 012005 (2015).

[12] Y. Taniyasu, M. Kasu, and T. Makimoto, "An aluminum nitride light-emitting diode with a wavelength of 210 nm," Nature **441**, 325–328 (2006).

[13] J. Glaab, J. Haefke, J. Ruschel, M. Brendel, J. Rass, T. Kolbe, A. Knauer, M. Weyers, S. Einfeldt, M. Guttmann, C. Kuhn, J. Enslin, T. Wernicke, and M. Kneissl, "Degradation effects of the active region in UV-C light-emitting diodes," J. Appl. Phys. **123**, 104502 (2018).

[14] Z. Bryan, I. Bryan, J. Xie, S. Mita, Z. Sitar, and R. Collazo, "High internal quantum efficiency in AlGaN multiple quantum wells grown on bulk AlN substrates," Appl. Phys. Lett. **106**, 142107 (2015).

[15] R. Gaska, Q. Fareed, G. Tamulaitis, I. Yilmaz, M. S. Shur, C. Chen, J. Yang, E. Kuokstis, A. Khan, J. C. Rojo, and L. J. Schowalter, "Stimulated emission at 258 nm in AlN/AlGaN quantum wells grown on bulk AlN substrates," MRS Proc. **764**, 69 (2003).

[16] H. Amano, R. Collazo, C. D. Santi, S. Einfeldt, M. Funato, J. Glaab, S. Hagedorn, A. Hirano, H. Hirayama, R. Ishii, Y. Kashima, Y. Kawakami, R. Kirste, M. Kneissl, R. Martin, F. Mehnke, M. Meneghini, A. Ougazzaden, P. J. Parbrook, S. Rajan, P. Reddy, F. Römer, J. Ruschel, B. Sarkar, F. Scholz, L. J. Schowalter, P. Shields, Z. Sitar, L. Sulmoni, T. Wang, T. Wernicke, M. Weyers, B. Witzigmann, Y.-R. Wu, T. Wunderer, and Y. Zhang, "The 2020 UV emitter roadmap," J. Phys. D: Appl. Phys. **53**, 503001 (2020).

[17] J. Glaab, J. Ruschel, T. Kolbe, A. Knauer, J. Rass, H. K. Cho, N. Lobo Ploch, S. Kreutzmann, S. Einfeldt, M. Weyers, and M. Kneissl, "Degradation of (In)AlGaN-based UVB LEDs and migration of hydrogen," IEEE Photonics Technol. Lett. **31**, 529–532 (2019).

[18] D. Monti, C. Santi, S. Ruos, F. Piva, J. Glaab, J. Rass, S. Einfeldt, F. Mehnke, J. Enslin, T. Wernicke, M. Kneissl, G. Meneghesso, E. Zanoni, and M. Meneghini, "High-current stress of UV-B (In)AlGaN-based LEDs: Defect-generation and diffusion processes," IEEE Trans. Electron Devices **66**, 3387 (2019).

[19] N. Trivellin, D. Monti, C. De Santi, M. Buffolo, G. Meneghesso, E. Zanoni, and M. Meneghini, "Current induced degradation study on state of the art DUV

LEDs," in *29th European Symposium on Reliability of Electron Devices, Failure Physics and Analysis (ESREF), 2018* [Microelectron. Reliab. **88-90**, 868–872 (2018)].
[20] J. Glaab, J. Ruschel, N. Lobo Ploch, H. K. Cho, F. Mehnke, L. Sulmoni, M. Guttmann, T. Wernicke, M. Weyers, S. Einfeldt, and M. Kneissl, "Impact of operation parameters on the degradation of 233 nm AlGaN-based far-UVC LEDs," J. Appl. Phys. **131**, 014501 (2022).
[21] V. Adivarahan, W. H. Sun, A. Chitnis, M. Shatalov, S. Wu, H. P. Maruska, and M. A. Khan, "250 nm AlGaN light-emitting diodes," Appl. Phys. Lett. **85**, 2175–2177 (2004).
[22] M. Meneghini, D. Barbisan, L. Rodighiero, G. Meneghesso, and E. Zanoni, "Analysis of the physical processes responsible for the degradation of deep-ultraviolet light emitting diodes," Appl. Phys. Lett. **97**, 143506 (2010).
[23] N. Trivellin, D. Monti, F. Piva, M. Buffolo, C. De Santi, E. Zanoni, G. Meneghesso, and M. Meneghini, "Degradation processes of 280 nm high power DUV LEDs: Impact on parasitic luminescence," Jpn. J. Appl. Phys. **58**, SCCC19 (2019).
[24] C.-t. Sah, R. Noyce, and W. Shockley, "Carrier generation and recombination in p-n junctions and p-n junction characteristics," Proc. IRE **45**, 1228–1243 (1957).
[25] H. Masui, S. Nakamura, and S. P. DenBaars, "Technique to evaluate the diode ideality factor of light-emitting diodes," Appl. Phys. Lett. **96**, 073509 (2010).
[26] J. M. Shah, Y.-L. Li, T. Gessmann, and E. F. Schubert, "Experimental analysis and theoretical model for anomalously high ideality factors ($n \gg 2.0$) in AlGaN/GaN *p-n* junction diodes," J. Appl. Phys. **94**, 2627–2630 (2003).
[27] H. Masui, "Diode ideality factor in modern light-emitting diodes," Semicond. Sci. Technol. **26**, 075011 (2011).
[28] D. Hollington, J. T. Baird, T. J. Sumner, and P. J. Wass, "Lifetime testing UV LEDs for use in the LISA charge management system," Classical Quantum Gravity **34**, 205009 (2017).
[29] OptanLED, TO-39 Ball Lens 250–280 nm UVC LED by Optan, https://www.optanled.com/products/optan-to-39-ball-lens (2020); accessed 01-12-2020.
[30] S. E. Technologies, TO-Can 39 Series (TUDx9H1B), http://www.s-et.com/upload2/TUD59H1B.PDF (2018); accessed 01-12-2020.
[31] D. Monti, M. Meneghini, C. De Santi, G. Meneghesso, E. Zanoni, J. Glaab, J. Rass, S. Einfeldt, F. Mehnke, J. Enslin, T. Wernicke, and M. Kneissl, "Defect-related degradation of AlGaN-based UV-B LEDs," IEEE Trans. Electron Devices **64**, 200–205 (2017).
[32] H. Inchauspé, T. Olatunde, S. Apple, S. Parry, B. Letson, N. Turetta, G. Mueller, P. J. Wass, and J. W. Conklin, "Numerical modeling and experimental demonstration of pulsed charge control for the space inertial sensor used in LISA," Phys. Rev. D **102**, 042002 (2020).
[33] T. Olatunde, "UV LED based charge control for the LISA gravitational reference sensor," Ph.D. thesis, University of Florida, 2018.